ACS Energy LETTERS

http://pubs.acs.org/journal/aelccp

Anisotropic Electrochemical Lithiation of Single Crystal Silicon Electrodes Assembled in an All-Solid-State Battery Configuration

Ridwan P. Putra, Daisuke Ito, Qin Si, Yusuke Morino, Kentaro Takase, and Takuya Masuda*

Cite This: *ACS Energy Lett.* 2025, 10, 6549−6556

Read Online

ACCESS | Metrics & More | Article Recommendations | Supporting Information

ABSTRACT: Electrochemical lithiation of single-crystal silicon (*c*-Si) electrodes with different surface orientations of (110), (100), and (111) was studied in an all-solid-state lithium-ion battery configuration. A lithium phosphorus oxynitride (LiPON) solid-electrolyte layer was sputter-deposited on the *c*-Si wafer, and a piece of Li metal foil was further incorporated to yield a solid-state half-cell with a configuration of *c*-Si/LiPON/Li. After electrochemical lithiation, their cross sections were analyzed using various techniques. Amorphous lithium silicide (*a*-Li_xSi) layers were generated at the *c*-Si/LiPON interface due to the insertion of lithium-ion from LiPON to *c*-Si lattices, followed by amorphization. Whereas *a*-$Li_{\sim1}Si$ was the predominant Li_xSi species in the lithiated Si(110) and (100), two distinct Li_xSi species, barely lithiated *a*-$Li_{\sim0}Si$ and almost fully lithiated *a*-$Li_{\sim3.4}Si$, formed in the lithiated Si(111) electrodes.

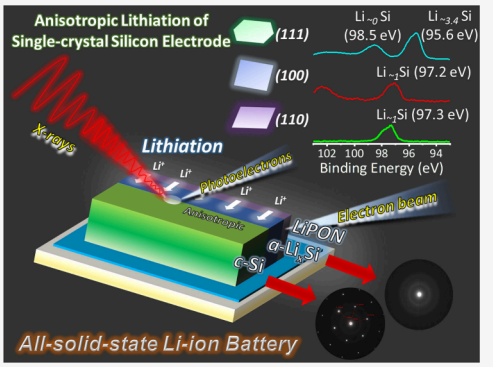

Silicon (Si) electrodes have garnered widespread interest as promising anode materials for lithium-ion batteries (LIBs) due to their exceptionally high theoretical energy density.[1] However, its significant volume changes during charge/discharge cycles can lead to unfavorable mechanical and electrochemical degradation.[2−4] Hence, it is critical to comprehensively understand the sequential physicochemical phenomena initiated by lithiation/delithiation, such as the diffusion of lithium-ions in Si and lithium silicide (Li_xSi), phase transformation, crack formation, pulverization and electrode failure to design highly durable Si-based anode materials and mitigate the mechanical deterioration that triggers premature electrode failure.[2−4] Recent advancements in X-ray computed tomography have enabled real-time monitoring of crack formation process within Si particles during charge and discharge cycles.[5−7] These developments have facilitated the understanding of the anisotropic crack formation mechanism induced by constraints arising in the densely packed and confined spaces between particles. Conversely, a comprehensive understanding of the multiscale chemomechanical degradation phenomena including lithium-ion insertion, crystalline structure transformations, volumetric changes, stress concentration, cracking, and pulverization necessitates elucidation of the anisotropic reaction mechanisms fundamentally based on the crystal structure of Si.

Single-crystal Si (*c*-Si) can be employed as an ideal model which allows us to track the anisotropic features and orientation-dependence of electrochemical lithiation/delithiation reactions by using different face orientations.[8−18] Numerous investigations have explored the lithiation behaviors of *c*-Si electrodes, especially when assembled in liquid-electrolyte LIB systems.[8−18] Among the various face orientations, the (110) surface is known to be more energetically favorable for Li-ion diffusion relative to the (100) and (111) surfaces, leading to a preferred volume expansion along the ⟨110⟩ direction.[9−12] Lee et al. (2011) studied the influence of electrochemical lithiation on the shape and volume expansion of *c*-Si nanopillar electrodes fabricated under different surface orientations.[19] They revealed a preferential volume expansion in the ⟨110⟩ direction compared to other directions, due to the rapid Li-diffusion channel along this direction.[19,20] In addition, a few groups independently predicted preferential Li-ion diffusion in the ⟨110⟩ directions.[21−23]

Recently, all-solid-state LIBs (ASSLIBs) are drawing considerable interest as the next-generation rechargeable batteries owing to their high chemical safety and wide

Received: August 12, 2025
Revised: November 5, 2025
Accepted: November 19, 2025

operating voltage window by substituting liquid organic electrolytes used in the conventional LIBs, with solid-electrolytes.[24−29] In contrast to the liquid-type LIBs where the continuous decomposition of liquid electrolyte occurs to form a solid electrolyte interphase (SEI) at the Si electrode surface newly exposed by volume changes, such continuous electrochemical decomposition of solid electrolyte is unlikely to occur during the operation of ASSLIBs. Thus, the use of Si anodes in ASSLIBs is deemed to be advantageous not only for practical applications but also for fundamental understanding of electrode processes as the impact of electrolyte decomposition would be less detrimental to the cell performance than those in conventional LIBs.[30−34] Taking this advantage, our group previously obtained the correlation between the X-ray photoelectron spectroscopy (XPS) peak position of Li_xSi in the Si 2p region and the electrochemical charge density, i.e., apparent Li content x determined excluding the electronic charge consumed for the decomposition of electrolyte, by *operando* XPS on a thin-film *a*-Si electrode in the ASSLIB configuration during electrochemical lithiation/delithiation.[35−37] In addition, we quantitatively analyzed the nanomechanical property, simultaneously with topography imaging, of a thin-film *a*-Si electrode by a bimodal atomic force microscopy technique.[38]

Unfortunately, however, most studies on the electrochemical lithiation mechanisms in *c*-Si focus mainly on liquid-type LIB systems, and their applications in ASSLIBs remain scarce. Therefore, the clarification and control of the anisotropic reaction/diffusion in *c*-Si with different surface orientations during electrochemical lithiation/delithiation, especially when assembled under ASSLIB configurations, are essential to achieve highly durable Si anodes with high energy density.[39,40] In this work, the electrochemical lithiation of *c*-Si electrodes with different surface orientations of (110), (100), and (111) was investigated in ASSLIB cells composed of *c*-Si wafer, Li metal foil, and sputter deposited lithium phosphorus oxynitride (LiPON) film. The microstructures and chemical species of the electrochemically lithiated electrodes were analyzed by scanning electron microscopy (SEM), energy-dispersive X-ray spectroscopy (EDS), transmission electron microscopy (TEM), selected area electron diffraction (SAED), and XPS.

The *c*-Si electrodes with different surface orientations of (110), (100), and (111) were used to construct ASSLIB cells, with a configuration of *c*-Si working electrode/LiPON solid-electrolyte layer/Li metal counter electrode (*c*-Si/LiPON/Li). Commercially available undoped *c*-Si wafers from Yamanaka Hutech Co., Ltd. with a resistivity of 1000 Ω·cm and thickness of 390 μm for the (110) surface, 540 μm for the (100) surface, and 525 μm for the (111) surface were used without any pretreatment. Radio frequency magnetron sputtering was employed to deposit the LiPON solid electrolyte layer with a thickness of ∼ 800 nm on the surface of a *c*-Si wafer using a commercial lithium phosphate (Li_3PO_4) target under an Ar/N_2 pressure of 0.4 Pa. The thickness and successful deposition of the LiPON layer were cross-checked by SEM after exposure of the cross sections of the samples. To produce ASSLIB cells with a configuration of *c*-Si/LiPON/Li, the *c*-Si/LiPON samples were combined with a piece of Li metal foil (Honjo Metal Co., Ltd.) with a thickness of 100 μm, as illustrated in Figure 1.

After prelithiation treatment under a current density of 0.5 μA cm^{-2} at 60 °C for 10 h, electrochemical lithiation was conducted at a current density of 1 μA cm^{-2} at 60 °C for each

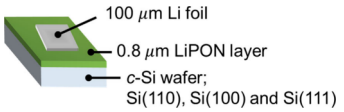

Figure 1. Configuration of the *c*-Si/LiPON/Li ASSLIB cells.

cell with a different face orientation, where the areal current density was determined based on the contact area between the LiPON layer and the Li metal foil. Typical galvanostatic voltage profiles of *c*-Si/LiPON/Li cells with different surface orientations of (110), (100), and (111) during electrochemical lithiation are shown in Figure S1. Microstructural characterizations were applied to the cross sections of the electrochemically lithiated *c*-Si electrodes exposed by cleavage.

The cross-sectional SEM-EDS mapping analysis results (JSM-7800F, JEOL Ltd., Japan equipped with an Aztec EDS system, Oxford Instruments, U.K.) of the electrochemically lithiated *c*-Si electrodes are shown in Figure 2. All of the P maps show a thin P layer with a thickness of ∼0.8 μm, indicating the presence of the LiPON solid-electrolyte layer. Notably, the Si maps indicate two layers with different Si atomic densities. The top layer in contact with LiPON layer and the bottom layer show a lower and higher atomic density of Si, respectively. It is reasonable to infer that the upper Si is the Li_xSi layer, where the atomic density of the Si layer decreases due to Li being inserted into the electrode during electrochemical lithiation. Meanwhile, the bottom Si layer with a higher Si atomic density is apparently the pristine (unreacted) *c*-Si layer.

In both the Si(110) and (100) electrodes, the generated Li_xSi and unreacted *c*-Si layers are clearly separated by a relatively smooth boundary. Interestingly, however, the boundary between the Li_xSi layer and *c*-Si in lithiated Si(111) is zigzag. The propagation of lithiation reaction in *c*-Si electrodes can be significantly affected by the preferential direction of Li diffusion such as ⟨110⟩,[9−12,19,20] the energy barriers of Li insertion,[23,42] and the mechanical stress.[13,43] Recently, Pan et al. investigated the anisotropic lithiation mechanism of *c*-Si with different surface orientations in contact with Li metal at high temperatures using the Reactive-Force-field based molecular dynamics (MD) simulations considering the mechanical stress and the elastic moduli of *c*-Si and Li−Si alloys as well as the energy barriers of Li insertion.[23] Their MD simulations clearly showed that the lithiation kinetics on Si(111) was much slower than those on the other surface orientations such as Si(110), (100) and (112), due to its very high energy barrier.[23] In our present study, the formation of Li_xSi with the zigzag boundary can be attributed to such extremely high energy barrier; Li was presumably inserted into the *c*-Si lattice from the defect sites such as the step-edges, strained Si at the native oxide/*c*-Si interface and protruding Li_xSi filaments (see below and SEM image of Figure 2(c)), followed by their diffusion in energetically more favorable directions, rather than propagating into the ⟨111⟩ direction through the extremely high energy barrier.

The lithiated Si(110) (Figure 2(a)) and (111) (Figure 2(c)) electrodes clearly show lines propagated almost parallel to or slightly tilted from the surface normal, which correlates with the proposed preferential Li-ion diffusion and lithiation directions, i.e., ⟨110⟩ (Figure 2(d−i)).[21−23] Judging from the contrast of SEM images of the lithiated Si(110) (Figure 2(a)) and (111) (Figure 2(c)) electrodes, the lines are considered to

https://doi.org/10.1021/acsenergylett.5c02573
ACS Energy Lett. 2025, 10, 6549−6556

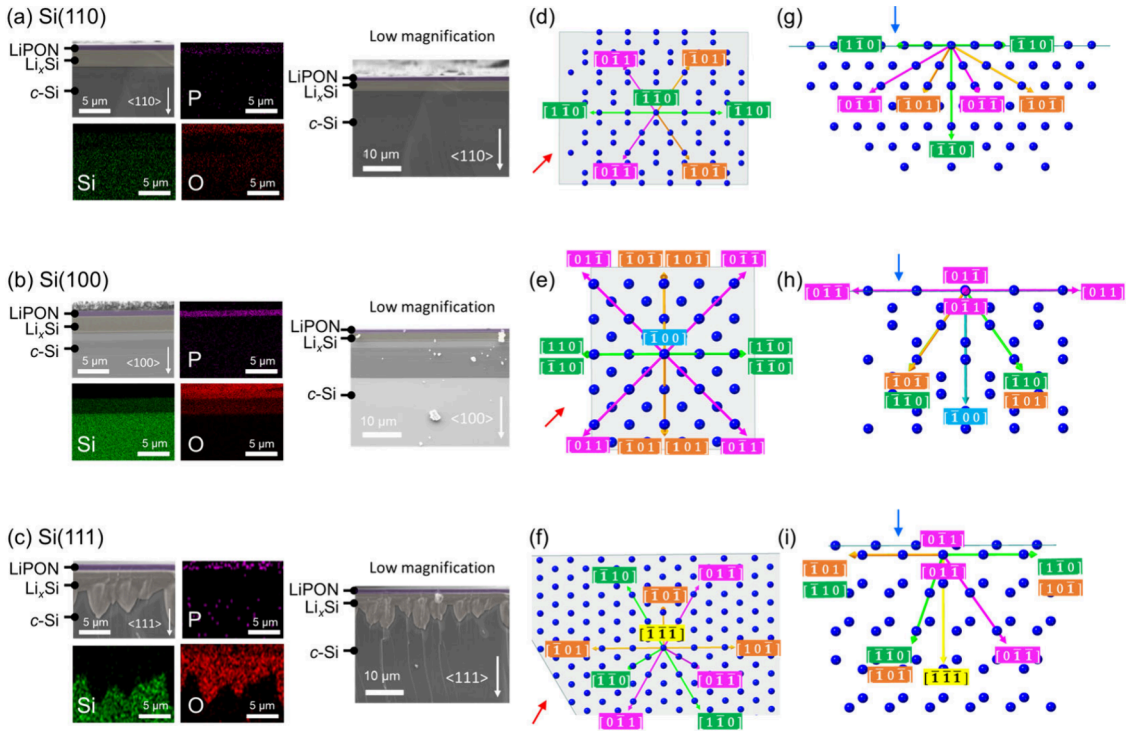

Figure 2. Cross-sectional SEM images and EDS maps of electrochemically lithiated *c*-Si electrodes: (a) Si(110), (b) Si(100), and (c) Si(111). (d–f) Top and (g–i) side views of the crystal structures of *c*-Si electrodes, projected in the directions of blue arrows in (g)–(i) and red arrows in (d)–(f), together with the ⟨110⟩ directions. In the SEM images, the boundaries of the LiPON, Li_xSi, and *c*-Si layers are highlighted with transparent planes. The crystal structures were generated by Crystal Maker (ver. 11.5, Crystal Maker Software, Ltd.), and the crystallographic information file of Si was obtained from Atom Work (NIMS, Japan).[41]

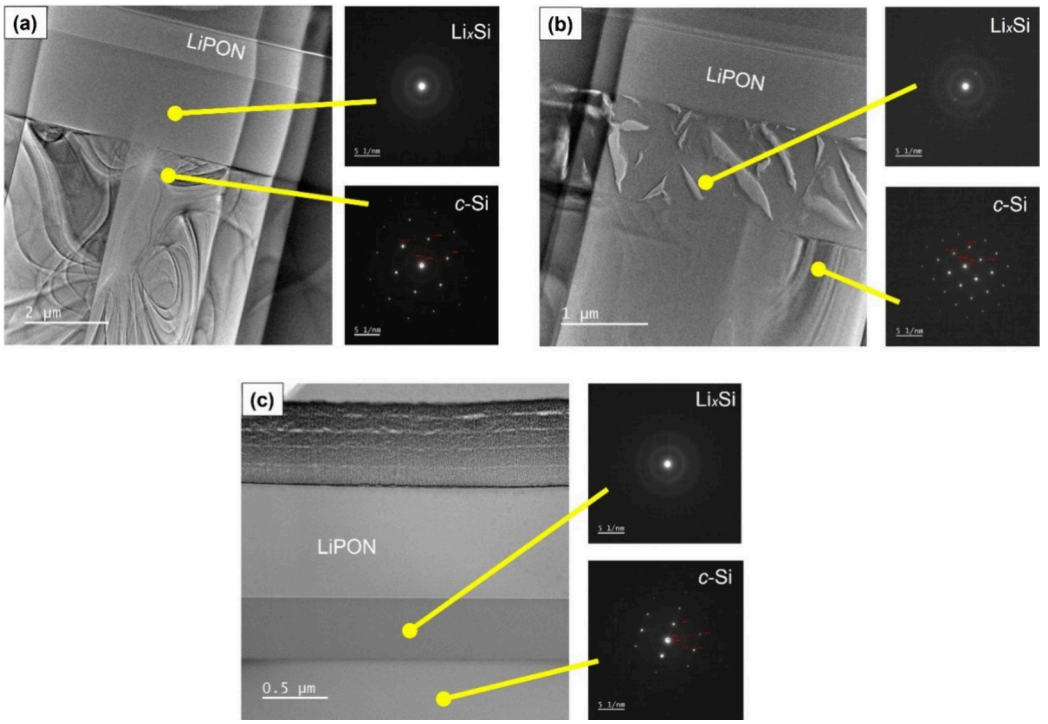

Figure 3. TEM images and electron diffraction patterns of the cross-section polished electrochemically lithiated *c*-Si electrodes: (a) Si(110), (b) Si(100), and (c) Si(111).

be Li_xSi filaments although it is unclear from the Si maps due to the insufficient pixel resolution. Such protrusion can be caused by the structural inhomogeneity of the LiPON/*c*-Si interfaces because the interfaces were formed by sputter deposition of LiPON layers on native *c*-Si surfaces without any

https://doi.org/10.1021/acsenergylett.5c02573
ACS Energy Lett. 2025, 10, 6549–6556

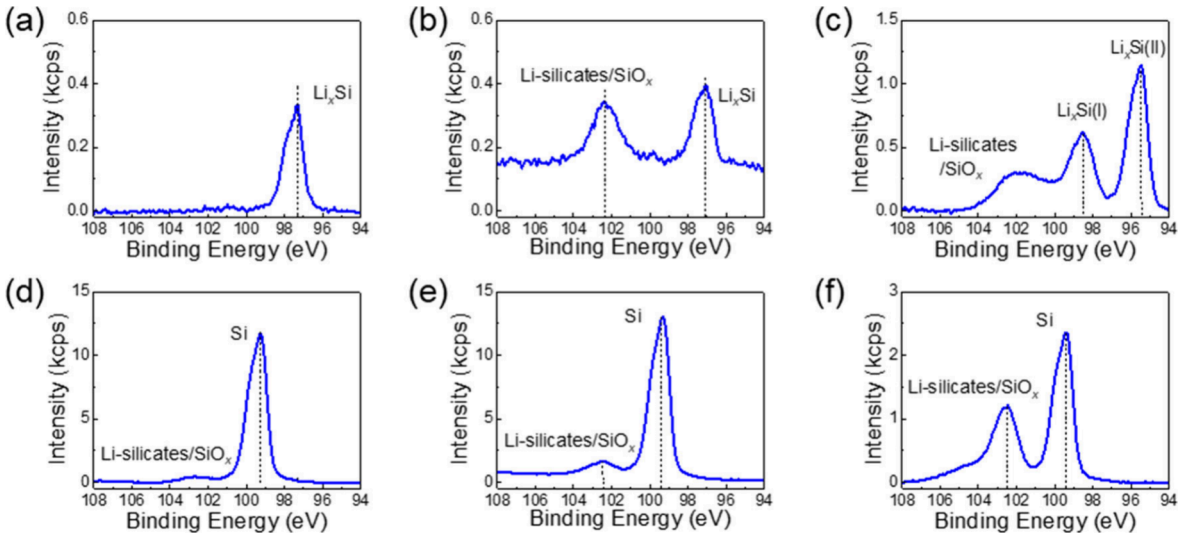

Figure 4. Typical photoelectron spectra in the Si 2p region of electrochemically lithiated *c*-Si electrodes in the areas (a, b, c) with and (d, e, f) without the Li$_x$Si layer: (a, d) Si(110), (b, e) Si(100), and (c, f) Si(111).

pretreatment such as wet chemical etching and hydrogen-termination.

In order to confirm the phase of the generated Li$_x$Si layer upon the electrochemical lithiation of the *c*-Si electrodes, TEM (JEM-ARM200F, JEOL Ltd., Japan) and scanning TEM (STEM) combined with EDS and SAED analyses were carried out on the cross sections of LiPON/Li$_x$Si/*c*-Si after being trimmed using a focused ion beam (SMF2000, Hitachi High-Tech Co., Japan). Figure 3 represents the TEM and SAED images of the polished cross sections, depicting the microstructural features and crystallographic information on the samples. Prior to the analysis, SEM-EDS mappings (Figure S2) were used to confirm the arrangement of the LiPON, Li$_x$Si, and *c*-Si layers, where the areas with low and high-Si atomic density in the Si map indicate the Li$_x$Si and *c*-Si layers, respectively. When electron diffractions were acquired at a position in the Li$_x$Si layers, halo ring patterns were identified (Figure 3). These signify that the Li$_x$Si layers are amorphous in all three lithiated *c*-Si electrodes.[44,45] Meanwhile, the unreacted *c*-Si layers were confirmed to be single-crystal, as indicated by the distinct and precisely delineated diffraction spots arranged in well-defined pattern.[44,45] A closer look on the electron diffraction images of the lithiated Si(100) electrode reveals, however, that the electron diffraction acquired on the Li$_x$Si layer indicates a halo ring pattern with a few discrete diffraction spots, suggesting that the predominant species is in the amorphous phase with small crystalline fractions, which can be related to the characteristics of electrochemical lithiation in the Si(100) surface and/or surface contamination during cross-section polishing by focused ion-beam.[13] The amorphous Li$_x$Si phase and *c*-Si lattice were distinctly identified by the variation in the contrast within the bright-field (BF) where the bright region typically indicates the compound consists of elements with lower atomic numbers, and the annular dark-field (ADF) STEM images where the dark region indicates the compound consists of elements with lower atomic numbers, as shown in Figure S3.[46,47]

XPS was used to determine the composition of Li$_x$Si formed in the lithiated *c*-Si electrodes. The measurements were carried out on a VersaProbe II (ULVAC-PHI, Japan) equipped with an Al−Kα source in the analysis chamber maintained at a basic pressure of about 6.0 × 10^{-8} Pa. Prior to acquiring the photoelectron spectra, X-ray-induced secondary electron images were obtained as shown in Figure S4, to position the focus of the X-ray beam on the area where the Li$_x$Si layer exists. Although the spatial resolution of the present laboratory-based XPS is fairly low (~100 μm), XPS measurements were conducted at a minimum of 10 analysis points at intervals of around ~20−50 μm to capture the Li$_x$Si layer in part of the field of view, as illustrated in Figure S5. The binding energies of the obtained spectra were calibrated with reference to the C 1s peak at 285 eV associated with hydrocarbon species.[48−51]

Figure 4 shows the typical Si 2p photoelectron spectra of the cross-section-exposed lithiated *c*-Si electrodes with and without peaks corresponding to the Li$_x$Si layer. In the cross-section of the lithiated Si(110) electrode, out of 10 spectra recorded at 10 analysis points, 9 spectra show two peaks corresponding to bulk Si^0 and silicon oxides/Li-silicates at ~99.3 and ~102.8 eV, respectively, as shown in Figure 4d and Figure S5a.[35−37,49,50] However, one of the spectra clearly shows a shift in the peak position associated with the Li$_x$Si species at ~97.3 eV (Figure 4a and Figure S5a). Based on our previous *operando* XPS study on the thin-film *a*-Si electrode during the first electrochemical lithiation/delithiation which correlates the position of Li$_x$Si peak in the Si 2p region and the apparent Li content *x* determined from the electrochemical charge density, the Li$_x$Si peak detected at ~97.3 eV is associated with the Li$_{\sim 1}$Si species.[35−37,49,50]

Likewise, the Li$_x$Si peak was also observed at ~97.2 eV in the photoelectron spectra of the lithiated Si(100) electrode in one of the spectra (Figure 4b and Figure S5b). Since the binding energy of the Li$_x$Si peak is very close to that in the lithiated Si(110) electrode (~97.3 eV), the composition of generated Li$_x$Si species should be almost identical, Li$_{\sim 1}$Si.[35−37,49,50] This suggests that the Li$_{\sim 1}$Si is thermodynamically favored to form in Si(110) and Si(100) during the electrochemical lithiation, which has been identified as one of the stable Li$_x$Si species cited in the literature.[52−57]

Unlike, two photoelectron spectra of the lithiated Si(111) electrode revealed two distinct Li$_x$Si peaks associated with coexisting two Li$_x$Si species (Figure 4c and Figure S5c). The

https://doi.org/10.1021/acsenergylett.5c02573
ACS Energy Lett. 2025, 10, 6549−6556

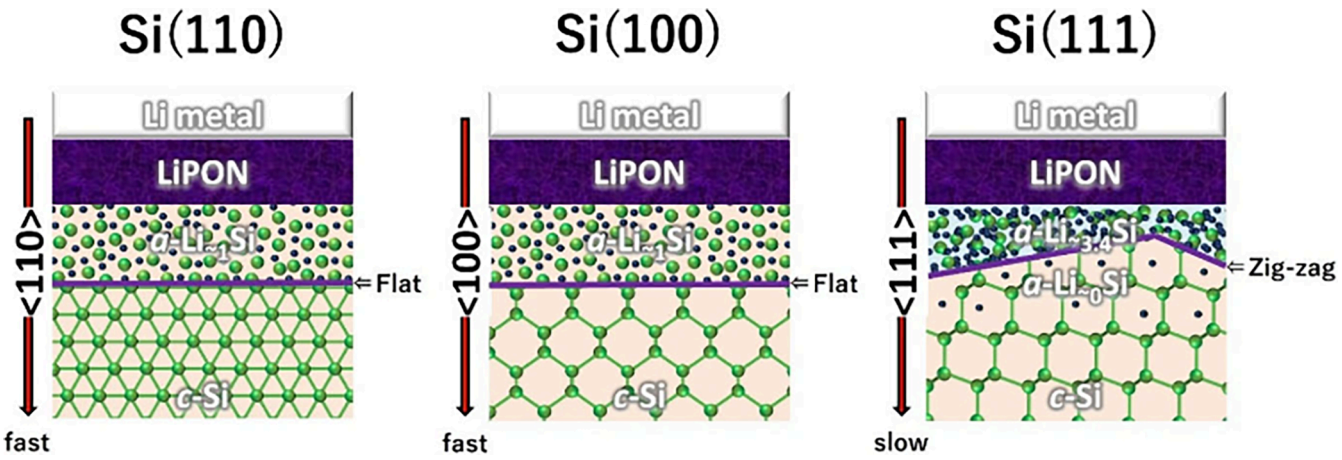

Figure 5. Proposed models of electrochemically lithiated *c*-Si electrodes with different surfaces of (110), (100), and (111) assembled in a *c*-Si/LiPON/Li ASSLIB cell configuration.

peak marked as Li_xSi(I), detected at a binding energy of ∼98.5 eV, was assignable to barely lithiated Li_xSi species, i.e., $Li_{\sim 0}Si$, and the other labeled as Li_xSi(II), identified at ∼95.6 eV, is attributed to almost fully lithiated $Li_{\sim 3.4}Si$ species.[35−37,49,50] Previously, Lee et al. performed a theoretical calculation study on the anisotropic diffusion of Li-ions using density functional theory and molecular dynamics.[14] They demonstrated that the migration of Li-ions into the interstitial sites of *c*-Si appeared to be the initial step of the lithiation, followed by the generation of a thin *c*-Li_xSi layer without altering the crystallinity of the *c*-Si.[14] The former barely lithiated Li_xSi(I) species could possibly be attributed to *c*-Si with Li-ions in the interstitial sites. Referencing our previous *operando* XPS study, it is considered that the generated Li_xSi(II) is composed of *a*-Li_xSi and metastable *c*-$Li_{15}Si_4$ phases, as clarified from the corresponding d*Q*/d*V* curve during electrochemical lithiation.[35−37,49,50]

From the comprehensive microstructural and surface chemical analysis of the electrochemically lithiated *c*-Si electrodes with different face orientations assembled in the *c*-Si/LiPON/Li ASSLIB configuration, the models for the electrochemical lithiation of the *c*-Si electrodes leading to the formation of *a*-Li_xSi compounds with different Li_xSi contents are proposed as shown in Figure 5.

In previous electrochemical lithium insertion studies using nanowires and nanoparticles that are not constrained by their surroundings, it has been reported that the reaction preferentially proceeds along the ⟨110⟩ direction.[19,58] In addition, the effect of lithiation-induced stress on the reaction propagation and boundary was also discussed both experimentally[59] and theoretically.[13] In the present case, the reaction boundary between *a*-$Li_{\sim 1}Si$ and *c*-Si is flat not only in the Si(110) (Figure 2a), which intersects perpendicularly with the ⟨110⟩ direction (Figure 2d,g), but also in the Si(100) (Figure 2b), which is parallel or at a 45° angle to the ⟨110⟩ direction (Figure 2e,h). In contrast, a zigzag reaction boundary is formed only in the Si(111) (Figure 2c), which is parallel or at a 35.26° angle to the ⟨110⟩ direction (Figure 2f,i). Thus, the formation of a zigzag reaction boundary cannot be explained solely by the correlation between the ⟨110⟩ direction and the crystal planes.

According to previous computational results, the lithiation reaction proceeds most readily along the ⟨110⟩ direction, and although it is slower, it also advances along the ⟨100⟩ direction.[23] On the other hand, the progression of the reaction along the ⟨111⟩ direction is significantly slower compared to the above two directions, due to a higher energy barrier for lithium insertion.[23] In the present system, none of the *c*-Si surfaces were pretreated, and it is considered that they are covered with a native oxide layer,[60] with strained silicon existing between the oxide layer and bulk silicon.[50−61,62] Furthermore, all the *c*-Si surfaces, including the Si(111), possess a slight deviation from the ideal face orientation due to the miscut angle, resulting in the existence of steps.[63,64] Even on the intrinsically lithium-insertion-resistant Si(111), it is thought that lithium insertion may occur at defect sites such as native oxides, strained silicon, and steps. Subsequently, the reaction may propagate in favorable directions corresponding to the orientation of these defect sites rather than along the ⟨111⟩ direction, leading to the formation of a zigzag reaction boundary as well as the formation of Li-rich $Li_{3.4}Si$.

The galvanostatic voltage profiles of the *c*-Si(110) and (100) electrodes during delithiation (Figure S6) showed behavior similar to that observed during delithiation from amorphous Li_xSi.[35,37] This suggests that delithiation from *a*-$Li_{\sim 1}Si$ formed in the *c*-Si(110) and (100) electrodes proceeds in a relatively reversible manner. In the cross-sectional SEM images of the *c*-Si(110) and (100) electrodes after lithiation and delithiation (Figure S7(a) and (b)), two distinct regions separated by flat reaction boundaries with different contrast can be clearly observed, suggesting that, in both the *c*-Si(110) and (100) electrodes, lithium is not completely removed from *a*-Li_xSi and *a*-Li_xSi does not revert to *c*-Si. In the case of the *c*-Si(111) electrode, the galvanostatic voltage curve (Figure S6) showed unstable voltage behavior from the early stage of delithiation. This instability may be caused by substantial volume changes during delithiation from Li-rich Li_xSi, resulting in local mechanical stress or strain effects. Even after delithiation, nonplanar reaction boundary remains between Li_xSi and *c*-Si in the SEM image (Figure S7(c)).

In summary, we have clarified the anisotropic reaction distribution of the electrochemical lithiation of *c*-Si electrodes with different face orientations in the ASSLIB configuration. Compared to the recent pioneering work by Na et al.,[20] the use of lower lithiation current density in our present work provides a few new insights. Upon lithiation, monocompositional *a*-$Li_{\sim 1}Si$ predominantly formed in the lithiated Si(110) and (100) electrodes with the smooth boundary from the unreacted *c*-Si, parallel to the surface, whereas two distinct Li_xSi, the $Li_{\sim 0}Si$ and $Li_{\sim 3.4}Si$ formed in the lithiated Si(111)

https://doi.org/10.1021/acsenergylett.5c02573
ACS Energy Lett. 2025, 10, 6549−6556

with the zigzag boundary from the *c*-Si. The formation of almost fully lithiated Si causes a phase transformation from crystalline $Li_{3.75}Si$ to amorphous Li_xSi during the successive delithiation,[35] which induces mechanical failures due to the accompanying significant volume changes.[38] In contrast, our present work shows that operating *c*-Si electrodes with (110) and (100) orientations with lower current density allows us to maintain the reaction progression at a certain composition, $Li_{\sim 1}Si$, thereby potentially suppressing mechanical failures caused by the phase transitions. Thus, not only the Li-ion diffusion and lithiation rate but also the reaction depth, i.e., lithium content in electrochemically generated Li_xSi, can be controlled by the face orientation for improved cycle life.

■ ASSOCIATED CONTENT

Supporting Information

The Supporting Information is available free of charge at https://pubs.acs.org/doi/10.1021/acsenergylett.5c02573.

Detailed sample preparation methods, conditions of electrochemical lithiation and typical galvanostatic voltage profiles of *c*-Si electrodes, analysis settings for SEM, TEM and XPS measurements, SEM images, EDS mappings, ADF and BF STEM images for TEM samples, typical optical images, X-ray induced secondary electron images, a series of Si 2p photoelectron spectra of cross sections of mechanically cleaved electrochemically lithiated *c*-Si electrodes, galvanostatic voltage profiles of *c*-Si electrodes during electrochemical lithiation and delithiation and cross-sectional SEM images of *c*-Si electrodes after electrochemical delithiation (PDF)

■ AUTHOR INFORMATION

Corresponding Author

Takuya Masuda − *Graduate School of Chemical Sciences and Engineering, Hokkaido University, Sapporo, Hokkaido 060-0810, Japan; Research Center for Energy and Environmental Materials (GREEN), National Institute for Materials Science (NIMS), Tsukuba, Ibaraki 305-0044, Japan;* orcid.org/0000-0001-7462-2177; Email: masuda.takuya@nims.go.jp

Authors

Ridwan P. Putra − *Graduate School of Chemical Sciences and Engineering, Hokkaido University, Sapporo, Hokkaido 060-0810, Japan; Research Center for Energy and Environmental Materials (GREEN), National Institute for Materials Science (NIMS), Tsukuba, Ibaraki 305-0044, Japan;* orcid.org/0000-0002-4941-4103

Daisuke Ito − *Murata Manufacturing Co., Ltd., Nagaokakyo, Kyoto 617-8555, Japan;* orcid.org/0009-0006-9296-1926

Qin Si − *Murata Manufacturing Co., Ltd., Nagaokakyo, Kyoto 617-8555, Japan*

Yusuke Morino − *Murata Manufacturing Co., Ltd., Nagaokakyo, Kyoto 617-8555, Japan;* orcid.org/0000-0002-6973-7786

Kentaro Takase − *Murata Manufacturing Co., Ltd., Nagaokakyo, Kyoto 617-8555, Japan*

Complete contact information is available at: https://pubs.acs.org/10.1021/acsenergylett.5c02573

Notes

The authors declare no competing financial interest.

■ ACKNOWLEDGMENTS

The authors acknowledge the financial support provided by the Center of Innovation NEXT Program (COI-NEXT) of Japan Science and Technology Agency (JST; Grant NumberJPMJPF2016). We also thank Mr. Kyosuke Matsushita, Ms. Makiko Oshida, Ms. Noriko Itoh, Mr. Keisuke Shinoda, and Mr. Kazuo Yamaguchi from the NIMS Battery Platform for technical assistance during sample characterizations.

■ REFERENCES

(1) Domi, Y.; Usui, H.; Sakaguchi, H. Analysis of the interfacial reaction between Si-based anodes and electrolytes in Li-ion batteries. *Chem. Commun.* **2024**, *60* (89), 12986−12999.

(2) Demirkan, M. T.; Trahey, L.; Karabacak, T. Cycling performance of density modulated multilayer silicon thin film anodes in Li-ion batteries. *J. Power Sources* **2015**, *273*, 52−61.

(3) Nakano, H.; Oh-ishi, K.; Matsubara, M. Tailoring the Void Space of a Silicon Anode for High-Capacity and Low-Expansion Lithium Storage. *Energy Technology* **2022**, *10* (11), No. 2200236.

(4) Ohta, N.; Kimura, S.; Sakabe, J.; Mitsuishi, K.; Ohnishi, T.; Takada, K. Anode Properties of Si Nanoparticles in All-Solid-State Li Batteries. *ACS Applied Energy Materials* **2019**, *2* (10), 7005−7008.

(5) Matsumoto, M.; Sakka, Y.; Zhong, C.; Shimoda, K.; Okazaki, K.-i.; Yamashige, H.; Ozeki, T.; Matsui, T.; Takeuchi, A.; Uesugi, M.; Uesugi, K.; Orikasa, Y. Operando Micro- and Nano-Computed Tomography Reveals Silicon−Electrolyte Interface Dynamics and Anisotropic Contact Loss in All-Solid-State Batteries. *ACS Nano* **2025**, *19* (41), 36527−36535.

(6) Morino, Y.; Takase, K.; Kanazawa, A.; Nagaoka, N.; Koshitani, N. In-Situ Internal Observation of Silicon Composite Anode in All-Solid-State Battery Using X-ray CT. *ACS Appl. Mater. Interfaces* **2025**, *17* (16), 23786−23794.

(7) Nelson, D. L.; Sandoval, S. E.; Pyo, J.; Bistri, D.; Thomas, T. A.; Cavallaro, K. A.; Lewis, J. A.; Iyer, A. S.; Shevchenko, P.; Di Leo, C. V.; McDowell, M. T. Fracture Dynamics in Silicon Anode Solid-State Batteries. *ACS Energy Letters* **2024**, *9* (12), 6085−6095.

(8) Aoki, N.; Omachi, A.; Uosaki, K.; Kondo, T. Structural Study of Electrochemically Lithiated Si(111) by using Soft X-ray Emission Spectroscopy Combined with Scanning Electron Microscopy and through X-ray Diffraction Measurements. *ChemElectroChem.* **2016**, *3* (6), 959−965.

(9) Kaghazchi, P. Mechanism of Li intercalation into Si. *Appl. Phys. Lett.* **2013**, *102* (9), No. 093901.

(10) Chan, M. K. Y.; Wolverton, C.; Greeley, J. P. First Principles Simulations of the Electrochemical Lithiation and Delithiation of Faceted Crystalline Silicon. *J. Am. Chem. Soc.* **2012**, *134* (35), 14362−14374.

(11) Zhang, Q.; Cui, Y.; Wang, E. Anisotropic Lithium Insertion Behavior in Silicon Nanowires: Binding Energy, Diffusion Barrier, and Strain Effect. *J. Phys. Chem. C* **2011**, *115* (19), 9376−9381.

(12) Baek, S.-H.; Park, J.-S.; Bae, E.-J.; Jeong, Y.-I.; Noh, B.-Y.; Kim, J. H. Influence of the crystallographic orientation of silicon nanowires in a carbon matrix on electrochemical performance as negative electrode materials for lithium-ion batteries. *J. Power Sources* **2013**, *244*, 515−520.

(13) Choi, Y. S.; Pharr, M.; Kang, C. S.; Son, S.-B.; Kim, S. C.; Kim, K.-B.; Roh, H.; Lee, S.-H.; Oh, K. H.; Vlassak, J. J. Microstructural evolution induced by micro-cracking during fast lithiation of single-crystalline silicon. *J. Power Sources* **2014**, *265*, 160−165.

(14) Choi, Y.-S.; Park, J.-H.; Ahn, J.-P.; Lee, J.-C. Interfacial Reactions in the Li/Si diffusion couples: Origin of Anisotropic Lithiation of Crystalline Si in Li−Si batteries. *Sci. Rep.* **2017**, *7* (1), No. 14028.

(15) Chamidah, N.; Suzuki, A.; Shimizu, T.; Zhong, C.; Shimoda, K.; Okazaki, K.-i.; Yaji, T.; Nakanishi, K.; Nishijima, M.; Kinoshita, H.; Orikasa, Y. Kinetic analysis of silicon−lithium alloying reaction in silicon single crystal using soft X-ray absorption spectroscopy. *RSC Adv.* **2023**, *13* (25), 17114−17120.

(16) Lin, H.; Noguchi, H.; Uosaki, K. Application of windowless energy dispersive spectroscopy to determine Li distribution in Li-Si alloys. *Appl. Phys. Lett.* **2018**, *112* (7), No. 073903.
(17) Lin, H.; Noguchi, H.; Uosaki, K. Effects of HF on the Lithiation Behavior of the Silicon Anode in $LiPF_6$ Organic Electrolyte Solution. *ACS Omega* **2020**, *5* (5), 2081−2087.
(18) Lin, H.; Uosaki, K.; Noguchi, H. Lithiation of the crystalline silicon as analyzed using soft X-ray emission spectroscopy and windowless energy dispersive X-ray spectroscopy. *Appl. Surf. Sci.* **2021**, *569*, No. 151040.
(19) Lee, S. W.; McDowell, M. T.; Choi, J. W.; Cui, Y. Anomalous Shape Changes of Silicon Nanopillars by Electrochemical Lithiation. *Nano Lett.* **2011**, *11* (7), 3034−3039.
(20) Na, I.; Kim, H.; Kunze, S.; Nam, C.; Jo, S.; Choi, H.; Oh, S.; Choi, E.; Song, Y. B.; Jung, Y. S.; Lee, Y. S.; Lim, J. Monolithic 100% Silicon Wafer Anode for All-Solid-State Batteries Achieving High Areal Capacity at Room Temperature. *ACS Energy Letters* **2023**, *8* (4), 1936−1943.
(21) Jung, H.; Lee, M.; Yeo, B. C.; Lee, K.-R.; Han, S. S. Atomistic Observation of the Lithiation and Delithiation Behaviors of Silicon Nanowires Using Reactive Molecular Dynamics Simulations. *J. Phys. Chem. C* **2015**, *119* (7), 3447−3455.
(22) Jung, S. C.; Choi, J. W.; Han, Y.-K. Anisotropic Volume Expansion of Crystalline Silicon during Electrochemical Lithium Insertion: An Atomic Level Rationale. *Nano Lett.* **2012**, *12* (10), 5342−5347.
(23) Pan, L.-Y.; Kuo, C.-L. Atomistic study on the origins of the anisotropic lithiation behaviors of the silicon anode using the reactive force field based molecular dynamics simulations. *Acta Mater.* **2024**, *265*, No. 119610.
(24) Iwama, T.; Ohnishi, T.; Masuda, T. Operando Observation of Lithiation and Delithiation Reactions of a $LiCoO_2$-Li_3BO_3 Composite Electrode Formed on a $Li_{6.6}La_3Zr_{1.6}Ta_{0.4}O_{12}$ Solid Electrolyte Sheet by Laboratory-based Hard X-ray Photoelectron Spectroscopy. *Electrochemistry* **2023**, *91* (11), 117005−117005.
(25) Sun, Y.-K. Promising All-Solid-State Batteries for Future Electric Vehicles. *ACS Energy Letters* **2020**, *5* (10), 3221−3223.
(26) Yue, L.; Ma, J.; Zhang, J.; Zhao, J.; Dong, S.; Liu, Z.; Cui, G.; Chen, L. All solid-state polymer electrolytes for high-performance lithium ion batteries. *Energy Storage Materials* **2016**, *5*, 139−164.
(27) Ichihara, F.; Niitsu, K.; Tanaka, Y.; Niwa, Y.; Mitsuishi, K.; Miyoshi, S.; Ohno, T.; Masuda, T. Structural Analysis of the $LiCoPO_4$ Electrode/NASICON-Type $Li_{1.3}Al_{0.3}Ti_{1.7}(PO_4)_3$ Solid Electrolyte Interface. *J. Phys. Chem. C* **2023**, *127* (31), 15043−15050.
(28) Ichihara, F.; Miyoshi, S.; Masuda, T. Co-sintering process of $LiCoO_2$ cathodes and NASICON-type LATP solid electrolytes studied by X-ray diffraction and X-ray absorption near edge structure. *Phys. Chem. Chem. Phys.* **2022**, *24* (42), 25878−25884.
(29) Tan, D. H. S.; Chen, Y.-T.; Yang, H.; Bao, W.; Sreenarayanan, B.; Doux, J.-M.; Li, W.; Lu, B.; Ham, S.-Y.; Sayahpour, B.; Scharf, J.; Wu, E. A.; Deysher, G.; Han, H. E.; Hah, H. J.; Jeong, H.; Lee, J. B.; Chen, Z.; Meng, Y. S. Carbon-free high-loading silicon anodes enabled by sulfide solid electrolytes. *Science* **2021**, *373* (6562), 1494−1499.
(30) Cheng, X.-B.; Zhang, R.; Zhao, C.-Z.; Wei, F.; Zhang, J.-G.; Zhang, Q. A Review of Solid Electrolyte Interphases on Lithium Metal Anode. *Advanced Science* **2016**, *3* (3), No. 1500213.
(31) Zhu, B.; Jin, Y.; Hu, X.; Zheng, Q.; Zhang, S.; Wang, Q.; Zhu, J. Poly(dimethylsiloxane) Thin Film as a Stable Interfacial Layer for High-Performance Lithium-Metal Battery Anodes. *Adv. Mater.* **2017**, *29* (2), No. 1603755.
(32) Zhou, W.; Wang, S.; Li, Y.; Xin, S.; Manthiram, A.; Goodenough, J. B. Plating a Dendrite-Free Lithium Anode with a Polymer/Ceramic/Polymer Sandwich Electrolyte. *J. Am. Chem. Soc.* **2016**, *138* (30), 9385−9388.
(33) Jiang, Z.; Xie, H.; Wang, S.; Song, X.; Yao, X.; Wang, H. Perovskite Membranes with Vertically Aligned Microchannels for All-Solid-State Lithium Batteries. *Adv. Energy Mater.* **2018**, *8* (27), No. 1801433.
(34) He, L.; Oh, J. A. S.; Watarai, K.; Morita, M.; Zhao, Y.; Sun, Q.; Sakamoto, T.; Lu, L.; Adams, S. Electromechanical Failure of NASICON-Type Solid-State Electrolyte-Based All-Solid-State Li-Ion Batteries. *Chem. Mater.* **2021**, *33* (17), 6841−6852.
(35) Endo, R.; Ohnishi, T.; Takada, K.; Masuda, T. Electrochemical Lithiation and Delithiation in Amorphous Si Thin Film Electrodes Studied by Operando X-ray Photoelectron Spectroscopy. *J. Phys. Chem. Lett.* **2022**, *13* (31), 7363−7370.
(36) Endo, R.; Ohnishi, T.; Takada, K.; Masuda, T. In Situ Observation of Lithiation and Delithiation Reactions of a Silicon Thin Film Electrode for All-Solid-State Lithium-Ion Batteries by X-ray Photoelectron Spectroscopy. *J. Phys. Chem. Lett.* **2020**, *11* (16), 6649−6654.
(37) Endo, R.; Ohnishi, T.; Takada, K.; Masuda, T. Instrumentation for tracking electrochemical reactions by x-ray photoelectron spectroscopy under conventional vacuum conditions. *Journal of Physics Communications* **2021**, *5* (1), No. 015001.
(38) Putra, R. P.; Matsushita, K.; Ohnishi, T.; Masuda, T. Operando Nanomechanical Mapping of Amorphous Silicon Thin Film Electrodes in All-Solid-State Lithium-Ion Battery Configuration during Electrochemical Lithiation and Delithiation. *J. Phys. Chem. Lett.* **2024**, *15* (2), 490−498.
(39) Bansal, A.; Bhandari, A.; Chakraborty, P.; Bhattacharya, J.; Pala, R. G. S. Alloying with Ge and Hollowing Reduces Lithiation-Induced Stresses in Si Nanopillar Anodes. *J. Electrochem. Soc.* **2020**, *167* (1), No. 013542.
(40) Wang, D.; Wang, Y.; Zou, Y.; Lu, C.; Ma, Z. Anisotropic mechanical properties of Si anodes in a lithiation process of lithium-ion batteries. *Acta Mechanica* **2018**, *229* (8), 3293−3303.
(41) Xu, Y.; Yamazaki, M.; Villars, P. Inorganic Materials Database for Exploring the Nature of Material. *Jpn. J. Appl. Phys.* **2011**, *50* (11S), No. 11RH02.
(42) Cubuk, E. D.; Wang, W. L.; Zhao, K.; Vlassak, J. J.; Suo, Z.; Kaxiras, E. Morphological Evolution of Si Nanowires upon Lithiation: A First-Principles Multiscale Model. *Nano Lett.* **2013**, *13* (5), 2011−2015.
(43) Zhao, K.; Pharr, M.; Wan, Q.; Wang, W. L.; Kaxiras, E.; Vlassak, J. J.; Suo, Z. Concurrent Reaction and Plasticity during Initial Lithiation of Crystalline Silicon in Lithium-Ion Batteries. *J. Electrochem. Soc.* **2012**, *159* (3), A238.
(44) Hirata, A.; Chen, M. Angstrom-beam electron diffraction of amorphous materials. *J. Non-Cryst. Solids* **2014**, *383*, 52−58.
(45) Moon, M. R.; Na, S.; Jeon, H.; An, C.-H.; Park, K.; Jung, D.; Kim, H.; Lee, Y.-B.; Lee, H.-J. Effects of Substrate Heating on the Amorphous Structure of InGaZnO Films and the Electrical Properties of Their Thin Film Transistors. *Applied Physics Express* **2010**, *3* (11), No. 111101.
(46) Hao, Y.; De Backer, A.; Findlay, S. D.; Van Aert, S. Towards atom counting from first moment STEM images: Methodology and possibilities. *Ultramicroscopy* **2025**, *268*, No. 114066.
(47) Oveisi, E.; Spadaro, M. C.; Rotunno, E.; Grillo, V.; Hébert, C. Insights into image contrast from dislocations in ADF-STEM. *Ultramicroscopy* **2019**, *200*, 139−148.
(48) Nagamura, N.; Konno, S.; Matsumoto, M.; Zhang, W.; Kotsugi, M.; Oshima, M.; Nouchi, R. Photoelectron spectromicroscopy analysis of graphene during gate-controlled photo-oxidation process. *Nano Express* **2022**, *3* (4), No. 044003.
(49) Masuda, T. Operando Analysis of Electrochemical Reactions in All-Solid-State Battery Using XPS. In *Interface Ionics: For All-Solid-State Batteries and Solid State Ionics Devices*; Iriyama, Y., Amezawa, K., Tateyama, Y., Yabuuchi, N., Eds.; Springer: Singapore, 2024; pp 299−310.
(50) Masuda, T.; Yoshikawa, H.; Noguchi, H.; Kawasaki, T.; Kobata, M.; Kobayashi, K.; Uosaki, K. In situ x-ray photoelectron spectroscopy for electrochemical reactions in ordinary solvents. *Appl. Phys. Lett.* **2013**, *103* (11), No. 111605.
(51) Seah, M. P. The quantitative analysis of surfaces by XPS: A review. *Surf. Interface Anal.* **1980**, *2* (6), 222−239.

https://doi.org/10.1021/acsenergylett.5c02573
ACS Energy Lett. 2025, 10, 6549−6556

(52) Morris, A. J.; Grey, C. P.; Pickard, C. J. Thermodynamically stable lithium silicides and germanides from density functional theory calculations. *Phys. Rev. B* **2014**, *90* (5), No. 054111.
(53) Artrith, N.; Urban, A.; Ceder, G. Constructing first-principles phase diagrams of amorphous Li_xSi using machine-learning-assisted sampling with an evolutionary algorithm. *J. Chem. Phys.* **2018**, *148* (24), No. 241711.
(54) Gu, M.; Wang, Z.; Connell, J. G.; Perea, D. E.; Lauhon, L. J.; Gao, F.; Wang, C. Electronic Origin for the Phase Transition from Amorphous Li_xSi to Crystalline $Li_{15}Si_4$. *ACS Nano* **2013**, *7* (7), 6303−6309.
(55) Shi, X.; Zhu, J.; Xia, Y.; Fan, F.; Zhang, F.; Gu, M.; Yang, H. Ultrahigh Malleability of the Lithiation-Induced Li_xSi Phase. *ACS Applied Energy Materials* **2018**, *1* (8), 4211−4220.
(56) Yao, H. R.; Wang, Z. Q.; Wu, M. S.; Liu, G.; Lei, X. L.; Xu, B.; Le, J. X.; Ouyang, C. Y. Lithium Ion Migration in Li-Si alloys: From First Principles Studies. *Int. J. Electrochem. Sci.* **2014**, *9* (4), 1854−1866.
(57) Tang, W. S.; Chotard, J.-N.; Janot, R. Synthesis of Single-Phase LiSi by Ball-Milling: Electrochemical Behavior and Hydrogenation Properties. *J. Electrochem. Soc.* **2013**, *160* (8), A1232.
(58) Yuk, J. M.; Seo, H. K.; Choi, J. W.; Lee, J. Y. Anisotropic Lithiation Onset in Silicon Nanoparticle Anode Revealed by in Situ Graphene Liquid Cell Electron Microscopy. *ACS Nano* **2014**, *8* (7), 7478−7485.
(59) Liu, X. H.; Fan, F.; Yang, H.; Zhang, S.; Huang, J. Y.; Zhu, T. Self-Limiting Lithiation in Silicon Nanowires. *ACS Nano* **2013**, *7* (2), 1495−1503.
(60) Morita, M.; Ohmi, T.; Hasegawa, E.; Kawakami, M.; Suma, K. Control factor of native oxide growth on silicon in air or in ultrapure water. *Appl. Phys. Lett.* **1989**, *55* (6), 562−564.
(61) Oh, J. H.; Yeom, H. W.; Hagimoto, Y.; Ono, K.; Oshima, M.; Hirashita, N.; Nywa, M.; Toriumi, A.; Kakizaki, A. Chemical structure of the ultrathin SiO_2/Si(100) interface: An angle-resolved Si 2p photoemission study. *Phys. Rev. B* **2001**, *63* (20), No. 205310.
(62) Watanabe, T.; Tatsumura, K.; Ohdomari, I. SiO_2/Si interface structure and its formation studied by large-scale molecular dynamics simulation. *Appl. Surf. Sci.* **2004**, *237* (1), 125−133.
(63) Matsuda, I.; Ueno, M.; Hirahara, T.; Hobara, R.; Morikawa, H.; Liu, C.; Hasegawa, S. Electrical Resistance of a Monatomic Step on a Crystal Surface. *Phys. Rev. Lett.* **2004**, *93* (23), No. 236801.
(64) Wei, J.; Wang, X. S.; Goldberg, J. L.; Bartelt, N. C.; Williams, E. D. Step-height mixtures on vicinal Si(111) surfaces. *Phys. Rev. Lett.* **1992**, *68* (26), 3885−3888.

https://doi.org/10.1021/acsenergylett.5c02573
ACS Energy Lett. 2025, 10, 6549−6556